Articles

A DFT Study toward the Mechanism of Chromium-Catalyzed Ethylene Trimerization

Werner Janse van Rensburg,*,† Cronjé Grové,† Jan P. Steynberg,‡ Klaus B. Stark,§ Johan J. Huyser,† and Petrus J. Steynberg*,†

Sasol Technology (Pty) Ltd, R&D Division, 1 Klasie Havenga Road, Sasolburg 9570, South Africa, Sasol Technology UK, Purdie Building, North Haugh St Andrews, Fife, Scotland, KY16 9ST, and Accelrys Inc., 1042 Kress Street, Houston, Texas 77020

Received October 3, 2003

A theoretical study of a mechanism for ethylene trimerization, catalyzed by Cr-pyrrolyl complexes, is proposed and investigated with density functional theory methods. The selective formation of 1-hexene is generally accepted to follow a metallacycle mechanism. A detailed spin state analysis for active species in the mechanism shows that the triplet spin state represents the ground spin state for all stationary points. Complete Gibbs free energy (298.15 K) surfaces are mapped for both η^5- and σ-bonding modes of pyrrole, as well as a stripped-down Cl anion model and a full $ClAlMe_3$ anion model. From the calculated results it is shown that the proposed metallacycle mechanism is energetically favorable, with metallacycle growth identified as the rate-determining step. In addition, it is demonstrated that different bonding modes of pyrrole are preferred at different stages in the proposed mechanism, effectively suggesting that ring slippage of the pyrrole occurs on the minimum energy path on the potential energy surface. From the calculated results important insight is gained into the hemilabile nature of the pyrrole ring in the mechanism, which in turn sheds light on the general requirements for an effective ligand in Cr-catalyzed ethylene trimerization.

Introduction

The transition metal catalyzed oligomerization of ethylene is traditionally used to synthesize α-olefins with product mixtures usually consisting of a mixture of even-numbered chain lengths (C_4−C_{26}).[1] The importance of α-olefins is realized from its application in the production of linear low-density polyethylene (LLDPE, C_6 and C_8), plasticizer and detergent alcohols (C_6−C_{16}), and synthetic lubricants.[2] Selective trimerization of ethylene to produce 1-hexene is highly desirable because it would avoid the production of unwanted olefins that conventional transition metal oligomerization processes produce. A lot of current interest is focused on the development of homogeneous catalyst systems to selectively trimerize ethylene. Cr-based catalysts are found to be especially well suited for the selective trimerization of ethylene, as is evident from a number of literature reports,[3−6] although Ti,[7] Ta,[8] and V[9] catalysis is also found to have application in this area.

Whereas the mechanism for ethylene oligomerization follows the standard Cossee−Arlman coordination/migratory insertion mechanism,[10] the selective conversion of ethylene to essentially 1-hexene is attributed to

* Corresponding authors. E-mail: Werner.JansevanRensburg@sasol.com; Petrie.Steynberg@sasol.com.
† Sasol Technology (Pty) Ltd.
‡ Sasol Technology UK.
§ Accelrys Inc.

(1) For examples, see: (a) Skupinska, J. *Chem. Rev.* **1991**, *91*, 613. (b) Keim, W.; Kowaldt, F. H.; Goddard, R.; Krüger, C. *Angew. Chem., Int. Ed. Engl.* **1978**, *17*, 466. (c) Svejda, S. A.; Brookhart, M. *Organometallics* **1999**, *18*, 65. (d) Killian, C. M.; Johnson, L. K.; Brookhart, M. *Organometallics* **1997**, *16*, 2005. (e) Mecking, S. *Coord. Chem. Rev.* **2000**, *203*, 325. (f) Ruther, T.; Braussaud, N.; Cavell, K. J. *Organometallics* **2001**, *20*, 1247. (g) Britovsek, G. J. P.; Mastroianni, S.; Solan, G. A.; Baugh, S. P. D.; Redshaw, C.; Gibson, V. C.; White, A. J. P.; Williams, D. J.; Elsegood, M. R. J. *Chem. Eur. J.* **2000**, *6*, 2221.

(2) Vogt, D. In *Applied Homogeneous Catalysis with Organometallic Compounds*; Cornils, B., Herrmann, W. A., Eds.; VCH: Weinheim, Germany, 1996; p 245.

(3) (a) Manyik, R. M.; Walker, W. E.; Wilson, T. P. *J. Catal.* **1977**, *47*, 197. (b) Yang, Y.; Kim, H.; Lee, J.; Paik, H.; Jang, H. G. *Appl. Catal. A* **2000**, *193*, 29. (c) Wasserscheid, P.; Grimm, S.; Köhn, R.; Haufe, M. *Adv. Synth. Catal.* **2001**, *343*, 814. (d) Carter, A.; Cohen, S. A.; Cooley, N. A.; Murphy, A.; Scutt, J.; Wass, D. F. *J. Chem. Soc., Chem. Commun.* **2002**, 858. (e) Monoi, T.; Sasaki, Y. *J. Mol. Catal. A: Chem.* **2002**, *187*, 135. (f) McGuinness, D. S.; Wasserscheid, P.; Keim, W.; Hu, C.; Englert, U.; Dixon, J. T.; Grove, C. *J. Chem. Soc., Chem. Commun.* **2003**, 334. (g) McGuinness, D. S.; Wasserscheid, P.; Keim, W.; Morgan, D.; Dixon, J. T.; Bollmann, A.; Maumela, H.; Hess, F.; Englert, U. *J. Am. Chem. Soc.* **2003**, *125*, 5272. (h) Morgan, D. H.; Schwikkard, S. L.; Dixon, J. T.; Nair, J. J.; Hunter, R. *Adv. Synth. Catal.* **2003**, 939. (i) Commereuc, D.; Drochon, S.; Saussine, L. (Institut Francais du Petrole) US Patent 6031145, 2000. (j) Wu, F.-J. (Amoco Corp.) US Patent 5811618, 1998. (k) Aoyama, T.; Mimura, H.; Yamamoto, T.; Oguri, M.; Koie, Y. (Tosoh Corp.) JP Patent 09176229, 1997.

(4) Briggs, J. R. *J. Chem. Soc., Chem. Commun.* **1989**, 674.

(5) (a) Reagan, W. K.; Pettijohn, T. M.; Freeman, J. W.; Benham, E. A. (Phillips Petroleum Co.)US Patent 5786431, 1998. (b) Lashier, M. E. (Phillips Petroleum Co.) EP 0780353A1, 1997.

(6) (a) Jolly, P. W. *Acc. Chem. Res.* **1996**, *29*, 544. (b) Emrich, R.; Heinemann, O.; Jolly, P. W.; Krüger, C.; Verhovnik, G. P. J. *Organometallics* **1997**, *16*, 1511.

10.1021/om0306269 CCC: $27.50
Publication on Web 02/17/2004

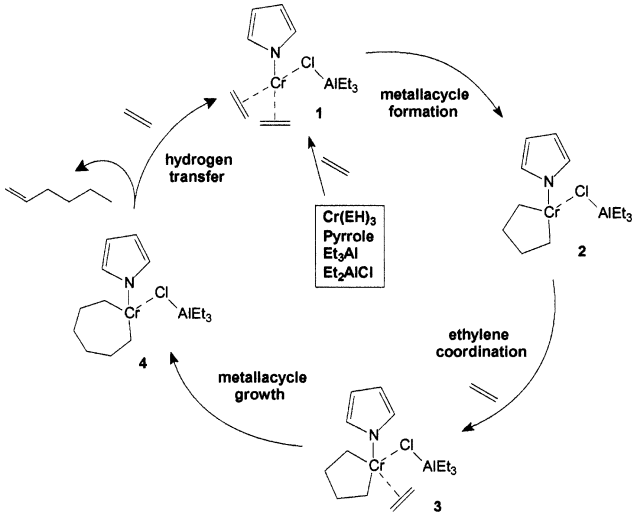

Figure 1. Proposed metallacycle mechanism for Cr-pyrrolyl-catalyzed trimerization of ethylene.

metallacycle intermediates.[4,6] Very recently proposed metallacycle mechanisms for Ti-[11] and Ta-catalyzed[12] ethylene trimerization were investigated with high-level density functional theory (DFT). To the best of our knowledge, however, no theoretical study of a possible Cr-catalyzed mechanism for ethylene trimerization has yet been reported. This is attributed to the lack of available fundamental experimental data on both the exact nature of Cr species in the catalytic cycle and the electronic structure of Cr complexes which require notoriously challenging open shell calculations.

In the present paper we propose and investigate an ethylene trimerization mechanism based on Cr-pyrrolyl complexes, which represents one of the most successful ethylene trimerization systems known (Phillips Petroleum Company).[5] Experimentally it is found that the combination of chromium tri(ethylhexanoate) [$Cr(EH)_3$], dimethylpyrrole, triethylaluminum, and diethylaluminum chloride yields a highly reactive ethylene trimerization system.[5] The proposed mechanism for ethylene trimerization with a pyrrole-based system is illustrated in Figure 1.[4,6]

Catalyst initiation is proposed to involve deprotonation of the pyrrole ligand, one-electron inner shell reduction of the Cr(III) in $Cr(EH)_3$, ligand exchange, anion formation, and coordination of two ethylene molecules to yield the neutral Cr(II) species, **1**, as the first active intermediate in the catalytic cycle. Alkylaluminum (TEA) activation of the Cr(III) catalyst precursor is believed to involve homolytic cleavage of a Cr−O bond through interaction of Al with the carbonyl oxygen of an ethylhexanoate fragment, as presented schematically in Figure 2. From this one-electron inner shell

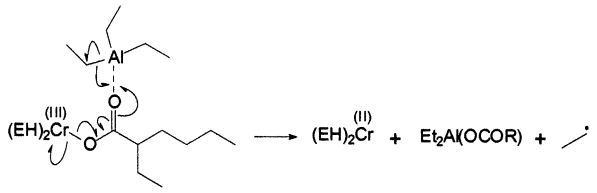

Figure 2. Proposed mechanism for Cr(III) activation by TEA.

reduction process an active Cr(II) species is generated together with a corresponding ethane radical.[13] A similar Cr(III) activation process involving interaction of $Cr(EH)_3$ with TEA, in the presence of an alternative ligand (2,6-diphenylphenol/anisole), is suggested in a very recent report by Morgan et al.[3h] In their work magnetic susceptibility measurements on the activated catalyst system showed μ_{eff} values of 5.17 and 3.61 μ_B in xylene and toluene, respectively, indicative of Cr(II) species. This effectively supports the suggestion that Cr(II) intermediates account for the initial activated catalytic species.

The anion fragment of **1** is proposed to consist of a $ClAlEt_3$ unit, or oligomer thereof,[3b] which remains coordinated throughout the mechanistic cycle. Metallacycle formation from **1** involves oxidative addition of the two ethylene fragments to yield a five-membered Cr(IV) metallacycle, **2**. This is followed by the coordination of a third ethylene molecule to yield **3**. Subsequent metallacycle growth results from insertion of the third ethylene molecule into the five-membered metallacyclic ring to yield the seven-membered metallacycle species **4**. The precedence for five- and seven-membered Cr metallacycles has been established by the isolation and characterization of crystal structures on related complexes.[6,14] 1-Hexene liberation is afforded by reductive eliminative intramolecular β-hydrogen migration to the ζ-carbon and regeneration of the active catalytic Cr(II) species, **1**, upon coordination of two ethylene molecules.

In this theoretical study high-level density functional theory is used to assess the validity of the proposed mechanism (Figure 1). Although a number of assumptions with regard to the mechanism are made, e.g., the presence of Cr(II) and Cr(IV) as active species in the mechanism and nature of the anionic fragment, it is believed that the proposed mechanism represents an acceptable hypothesis suitable as a thorough first attempt to theoretically investigate a Cr-catalyzed ethylene trimerization mechanism. In addition to the mapping of the potential energy surface (PES) of the proposed mechanism a number of additional fundamental aspects are also addressed, e.g., the preferred spin state of various Cr species, the influence of coordination mode of the pyrrole ligand, nature of the anionic

(7) (a) Deckers, P. J. W.; Hessen, B.; Teuben, J. H. *Angew. Chem., Int. Ed.* **2001**, *40*, 2516. (b) Deckers, P. J. W.; Hessen, B.; Teuben, J. H. *Organometallics* **2002**, *21*, 5122. (c) Pellechia, C.; Pappalardo, D.; Oliva, L.; Mazzeo, M.; Gruter, G.-J. *Macromolecules* **2000**, *33*, 2807.

(8) Andes, C.; Harkins, S. B.; Murtuza, S.; Oyler, K.; Sen, A. *J. Am. Chem. Soc.* **2001**, *123*, 7423.

(9) Santi, R.; Romano, A. M.; Grande, M.; Sommazzi, A.; Masi, F.; Proto, A. (ENICHEM S.P.A.) WO 0168572, 2001.

(10) (a) Cossee, P. *J. Catal.* **1964**, *3*, 80. (b) Arlman, E. J.; Cossee, P. *J. Catal.* **1964**, *3*, 99.

(11) (a) Blok, A. N. J.; Budzelaar, P. H. M.; Gal, A. W. *Organometallics* **2003**, *22*, 2564. (b) de Bruin, T. J. M.; Magna, L.; Raybaud, P.; Toulhout, H. *Organometallics* **2003**, *22*, 3404.

(12) Yu, Z.-X.; Houk, K. N. *Angew. Chem., Int. Ed.* **2003**, *42*, 808.

(13) From unpublished in-house experimental studies on the Cr-pyrrolyl catalyst system the following observations are made for catalyst activation: (i) During TEA/$Cr(EH)_3$ catalyst activation a gaseous white haze is observed as part of the reaction mixture. Although not analyzed as such, it is strongly believed that this observation is explained by the formation of butane gas resulting from the coordination of two ethane radical species, which is in turn formed during the activation process. (ii) During activation a distinct color change from green to brown is observed, in line with a Cr(III) to Cr(II) oxidation state change.

(14) Bercaw, J. E. The 15th International Symposium on Olefin Metathesis and Related Chemistry (ISOM XV) July 28−Aug 1, 2003, Kyoto, Japan.

fragment, conformations of the metallacycle rings, and charge distribution effects.

Computational Details

For most equilibrium structures preliminary geometries were optimized by using the PM3[15] semiempirical Hamiltonian available in Spartan'02 (Wavefunction Inc.).[16] This approach ensured the rapid scanning of the preliminary PES and provided reasonable starting geometries for higher level DFT calculations. All final geometry optimizations were performed with the DMol^3 density functional theory (DFT) code[17] as implemented in the MaterialsStudio (Version 2.1.5) program package of Accelrys Inc. The nonlocal generalized gradient approximation (GGA) functional by Perdew and Wang (PW91)[18] was used for all geometry optimizations. The convergence criteria for these optimizations consisted of threshold values of 2×10^{-5} Ha, 0.00189 Ha/Å, and 0.00529 Å for energy, gradient, and displacement convergence, respectively, while a self-consistent-field (SCF) density convergence threshold value of 1×10^{-6} Ha was specified. DMol^3 utilizes a basis set of numeric atomic functions, which are exact solutions to the Kohn−Sham equations for the atoms.[19] These basis sets are generally more complete than a comparable set of linearly independent Gaussian functions and have been demonstrated to have small basis set superposition errors.[19] In the present study a polarized split valence basis set, termed double numeric polarized (DNP) basis set, has been used. All geometry optimizations employed highly efficient delocalized internal coordinates.[20] The use of delocalized coordinates significantly reduces the number of geometry optimization iterations needed to optimize larger molecules compared to the use of traditional Cartesian coordinates.

All the geometries optimized were also subjected to full frequency analyses at the same GGA/PW91/DNP level of theory to verify the nature of all stationary points. Equilibrium geometries were characterized by the absence of imaginary frequencies. Preliminary transition state geometries were obtained by either the DMol^3 PES scan functionality in Cerius^2 (Version 4.8, Accelrys, Inc.) or the integrated linear synchronous transit/quadratic synchronous transit (LST/QST) algorithm[21] available in MaterialsStudio. These preliminary structures were then subjected to full TS optimizations using an eigenvector following algorithm. For selected transition state geometries confirmation calculations, involving intrinsic reaction path (IRP)[22] calculations, were performed in which the path connecting reagent, TS, and product are mapped. The IRP calculations, performed at the same GGA/PW91/DNP level of theory, ensured the direct connection of transition states with the respective reactant and product geometries. All IRP calculations performed are referred to in the text. All transition structure geometries exhibited only one imaginary frequency in the reaction coordinate. All reported energies refer to Gibbs free energy corrections to the total electronic energies at 298.15 K with the inclusion of zero-point energy (ZPE) corrections, unless explicitly stated to the contrary.

A comprehensive analysis of preferred multiplicity of Cr for selected Cr(II) and Cr(IV) complexes, including representative examples for both equilibrium and transition state geometries, was performed by conducting open shell calculations for electrons in the excited states. For singlet structures closed shell optimizations were performed. The three possible spin states of Cr(II) complexes (singlet, triplet, and quintet) and two spin states for Cr(IV) complexes (singlet and triplet) were considered. From this analysis (discussed in detail in the Results and Discussion section) a preferred triplet spin state for stationary points in the proposed mechanistic cycle (consisting of only Cr(II) and Cr(IV) species) was established, in agreement with the tendency of Cr to exhibit high spin states. Consequently, unrestricted triplet spin states were specified for all geometry optimizations unless explicitly stated to the contrary.

Self-consistent-field (SCF) convergence problems are frequently encountered for open shell organometallic systems. To enhance SCF convergence efficiency during optimization of stationary points, a small electron thermal smearing value of 0.005 Ha was specified for all calculations unless explicitly stated to the contrary. The thermal smearing option in MaterialsStudio makes use of a fractional electron occupancy scheme at the Fermi level according to a finite-temperature Fermi function.[23,24] The application of this technique was justified by the relatively similar energy differences and geometries obtained for reference calculations in which smearing and no smearing were used. Population analysis (Hirshfeld charges) was performed for GGA/PW91/DNP optimized structures at the same level of theory.[25]

Results and Discussion

Ligand Coordination Mode. Throughout this study pyrrole is used as model ligand for 2,5-dimethylpyrrole commonly used in experimental studies.[26] Pyrrole can theoretically coordinate in a number of ways to a metal center, including pentahapto (η^5), trihapto (η^3), and sigma (σ) bonding (with a covalent Cr−N interaction) modes. In the η^5-bonding mode the ligand acts as a tridentate ligand, contributing six electrons to the coordination sphere of Cr, while the σ-bonding mode is monodentate, contributing only two electrons to the valence shell. Therefore, species **1** and **3** in Figure 1 are 16-electron complexes for η^5-pyrrole and 12-electron complexes for σ-pyrrole, whereas **2** and **4** in Figure 1 are 14-electron complexes for η^5-pyrrole and 10-electron complexes for σ-pyrrole. It is thus evident that the bonding mode of pyrrole will dictate the valence electron count in the active catalytic species. For all complexes optimized in this study the η^5- and σ-bonding modes of pyrrole, which represents the two most likely extremes for bonding of pyrrole,[27] were explicitly considered to assess the preferred ligand bonding modes of the relevant complexes.

(15) Stewart, J. J. P. *J. Comput. Chem.* **1989**, *10*, 209.
(16) Wavefunction, Inc.: 18401 Von Karman Avenue, Suite 370, Irvine, CA 92612.
(17) (a) Delley, B. *J. Chem. Phys.* **1990**, *92*, 508. (b) Delley, B. *J. Phys. Chem.* **1996**, *100*, 6107. (c) Delley, B. *J. Chem. Phys.* **2000**, *113*, 7756.
(18) Perdew, J. P.; Wang, Y. *Phys. Rev.* **1992**, *B45*, 13244.
(19) Delley, B. *Density Functional Theory: A Tool for Chemistry*; Seminario, J. M., Politzer, P., Eds.; Elsevier: Amsterdam, The Netherlands, 1995.
(20) Andzelm, J.; King-Smith, R. D.; Fitzgerald, G. *Chem. Phys. Lett.* **2001**, *335*, 321.
(21) Govind, N.; Petersen, M.; Fitzgerald, G.; King-Smith, D.; Andzelm, J. *Comput. Mater. Sci.* (accepted for publication).
(22) The IRP technique used in MaterialsStudio (Accelrys Inc., Version 2.1.5) also corresponds to the intuitive minimum energy pathway (MEP) connecting two structures and is based on the nudged-elastic band (NEB) algorithm of Henkelman and Jonsson: Henkelman, G.; Jonsson, H. *J. Chem. Phys.* **2000**, *113*, 9978.
(23) Delley, B. In *Modern Density Functional Theory: A Tool for Chemistry*; Seminario, J. M., Politzer, P., Eds.; Theoretical and Computational Chemistry, Vol. 2, Elsevier: Amsterdam, The Netherlands, 1995.
(24) Weinert, M.; Davenport, J. W. *Phys. Rev. B* **1992**, *45*, 13709.
(25) (a) Hirshfeld, F. L. *Theor. Chim. Acta B* **1977**, *44*, 129. (b) Delley, B. *Chem. Phys. Lett.* **1986**, *110*, 329.
(26) It was found from in-house experimental studies that ethylene trimerizatrition runs with pyrrole as ligand behave similarly compared to 2,5-dimethylpyrrole.
(27) Reagan, W. K. Symposium on novel preparation and conversion of light olefins presented before the Division of Petroleum Chemistry, Inc., American Chemical Society, Miami Beach meeting, Sept 10−15, 1989.

Multiplicity. Coordination compounds containing soft π-acidic ligands (e.g., Cp-, pyrrole-anions, etc.) are often found in low oxidation states, where the strongly covalent metal−ligand interactions typically enforce the 18-electron rule and a spin-paired ground state. Cr(0), with its $3d^5 4s^1$ valence shell, as well as the different oxidation states of Cr (Cr^{1+}−Cr^{5+}), exhibit unpaired electrons in the valence shell, and the associated paramagnetism makes NMR characterization of Cr complexes impractical. Organometallic complexes of this nature, sometimes also referred to as "metallaradicals", are notoriously difficult to accommodate computationally due to SCF convergence problems often encountered, as well as the computationally expensive nature of open shell calculations. These phenomena are probably the reasons that theoretical studies based on Cr chemistry are less frequently encountered compared to other transition metals.

The relevance of electron pairing energy as a possible destabilizing factor for ligand coordination to Cr was addressed in open shell computational studies (MP2 and DFT) by Cacelli et al.[28] In their work it was pointed out that in the presence of an additional PH_3 donor, which will exert a favorable "chelate effect", 22.5 kcal/mol is needed to promote the quartet ground state 15-electron complex, $CpCr^{(III)}Cl_2(PH_3)$, to the doublet excited state (i.e., vacating a singly occupied valence shell orbital), while only 16.5 kcal/mol is gained upon formation of the doublet 17-electron complex, $CpCr^{(III)}Cl_2(PH_3)_2$, from the doublet 15-electron precursor, $CpCr^{(III)}Cl_2(PH_3)$. This shows that the energy gained upon donor ligand coordination is not sufficient to overcome the electron pairing energy of the Cr(III) center. In more recent calculations[29] the importance of spin state crossing during the reaction of transition metal compounds is emphasized. These spin crossing phenomena are also referred to as two-state reactivity (TSR)[30] involving participation of spin inversion at transition states. From these studies it is clear that consideration of all possible spin states of a transition metal center is essential to ensure that when spin state crossing does occur, the minimum energy crossing point (MECP) has been obtained. MECPs are particularly important when equilibrium structures for reagents and products have different spin states and when transition state geometries exhibit different spin states, on the lowest energy path, compared to reagents and/or products. Obtaining experimental evidence for spin state crossings would require spin state measurements of intermediates, a challenging[29] aspect that has not been conducted successfully yet. Therefore, spin state crossings are more conveniently addressed by a computational approach.[29,30] From these studies it was observed that the nature of the exchange part of the DFT functional strongly influences the accuracy of the computed spin state splittings, which is particularly strong for the first-row transition metals (Sc−Cu) with presumably large exchange interactions between the compact 3d orbitals of these metals. Consequently, the identification of the ground spin states for the different Cr(II) and Cr(IV) equilibrium and transition state geometries in our study is essential to ensure the location of the lowest energy stationary points on the calculated PESs. Currently, methodology to accurately compute MECP energies for open shell transition metal complexes is not available in MaterialsStudio (see Computational Details), and we have opted for a manual approach to determine whether Cr spin state is conserved or altered during the catalytic cycle. Five model stationary points in the proposed mechanistic cycle (Figure 1) were identified as representative structures for the spin state analysis, viz., the Cr(II) ethylene coordination complex (**M1**), the Cr(IV) five-membered metallacycle (**M2**), the direct Cr(IV) seven-membered metallacycle product (**M3**), the transition structure for metallacycle formation (**M1**−**2**), and the transition structure for metallacycle growth (**M2**−**3**), illustrated in Figure 3.

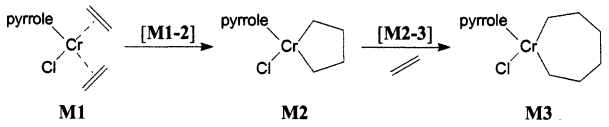

Figure 3. Equilibrium and transition state geometries considered in multiplicity analysis.

The selected transition state geometries represent examples of both a change of oxidation state of Cr [from Cr(II) to Cr(IV), **M1**−**2**] and conservation of oxidation state of Cr [(Cr(IV), **M2**−**3**] during the respective transformations. Both η^5- and σ-bonding modes of pyrrole were explicitly considered for all five geometries. For the Cr(II) complexes, **M1** and **M1**−**2**, three spin states (singlet, triplet, and quintet) were considered, while two spin states (singlet and triplet) were considered for the Cr(IV) species, **M2**, **M2**−**3**, and **M3**, effectively representing all possible multiplicities. Full equilibrium and transition state geometry optimizations were performed both without fractional occupation (no smearing) of orbitals at the Fermi level and with specifying a thermal smearing range of 0.005 Ha to yield a total of 48 geometry optimizations.[31] The relative calculated electronic energies for the different spin states of these optimized geometries are summarized in Table 1.

From the relative values in Table 1 it is evident that the triplet spin state represents the ground state for all equilibrium and transition state geometries considered. No structure for η^5-pyrrole quintet **M1** could successfully be optimized in which it was found that both ethylene molecules spontaneously drift away from the Cr center during optimization. This result is not surprising since the number of available coordination sites in η^5-pyrrole **M1** is exceeded by 1 (assuming a preferred octahedral 6 site arrangement) in the high quintet spin state, effectively eliminating the possibility for the proposed structure to exist. The smallest difference in relative spin state energies is found for the σ-pyrrole **M1** geometry in which the singlet structure is 2.9 kcal/mol

(28) (a) Cacelli, I.; Keogh, D. W.; Poli, R.; Rizzo, A. *New J. Chem.* **1997**, *21*, 133. (b) Cacelli, I.; Keogh, D. W.; Poli, R.; Rizzo, A. *J. Phys. Chem. A* **1997**, *101*, 9801.

(29) (a) Poli, R.; Harvey, J. N. *Chem. Soc. Rev.* **2003**, *32*, 1. (b) Green, J. C.; Harvey, J. N.; Poli, R. *J. Chem. Soc., Dalton Trans.* **2002**, 1861. (c) Harvey, J. N.; Aschi, M.; Schwarz, H.; Koch, W. *Theor. Chem. Acc.* **1998**, *99*, 95.

(30) Schröder, D.; Shaik, S.; Schwarz, H. *Acc. Chem. Res.* **2000**, *33*, 139.

(31) Although not alluded to here, subtle differences in geometrical parameters for complexes optimized at different spin states were found. Coordinates for all these geometries optimized at different spin states are included in the Supporting Information.

Table 1. Relative Electronic Energies for Different Spin States of M1, M1−2, M2, M2−3, and M3 in kcal/mol (values in parentheses are calculated with a thermal smearing range of 0.005 Ha)

		M1	M1−2	M2	M2−3	M3
η^5-pyrrole	singlet	16.4 (15.1)	9.9 (9.3)	15.2 (14.1)	17.1 (14.9)	12.2 (11.5)
	triplet	0.0 (0.0)	0.0 (0.0)	0.0 (0.0)	0.0 (0.0)	0.0 (0.0)
	quintet	*a*	25.9 (25.9)			
σ-pyrrole	singlet	2.9 (2.9)	15.7 (11.5)	19.4 (17.8)	10.6 (10.5)	*b* (15.7)
	triplet	0.0 (0.0)	0.0 (0.0)	0.0 (0.0)	0.0 (0.0)	0.0 (0.0)
	quintet	3.5 (3.4)	*b* (22.0)			

[a] No structure could successfully be optimized for quintet **M1** due to the lack of sufficient coordination sites on Cr(II) in the highest quintet spin state. In all efforts both ethylene molecules spontaneously drifted away from the Cr center. [b] SCF did not converge when no smearing was specified.

higher and the quintet structure 3.5 kcal/mol higher in energy compared to the triplet geometry. In all the other cases the alternative spin states were significantly higher in energy (10.6−25.9 kcal/mol) compared to the preferred triplet geometries. Relative energies obtained for the quintet transition structures, **M1−2**, were found to be significantly higher in energy compared to both the singlet and triplet optimized geometries, effectively showing that the highest spin state does not necessarily represent the most favored spin state for Cr complexes. Geometry optimizations for the singlet σ-pyrrole complex **M3** and the quintet σ-pyrrole transition structure **M1−2**, as indicated in Table 1, could not successfully be optimized when integer values for orbital occupations of electrons at the Fermi level (no smearing) were enforced. In both cases the SCF iterations did not converge. However, it is evident from the relative energies calculated for fractional electron occupation at the Fermi level (0.005 Ha smearing) that the triplet spin state prevails as ground state throughout. A general comparison of relative spin state energies calculated for all species in Table 1 shows that essentially small differences are found between relative energies obtained with (0.005 Ha) and without smearing. From this multiplicity analysis we thus conclude that in our study a triplet spin state is conserved throughout the proposed mechanistic cycle. Furthermore, the use of a thermal smearing range of 0.005 Ha was found to yield energy differences similar to the energies where no smearing was specified, effectively prompting the use of thermal smearing for all geometry optimizations discussed in the remainder of this paper. This strategy ensured the efficient convergence of SCF iterations for all geometry optimizations conducted.

Geometries. For the calculated ethylene trimerization mechanistic cycle two bonding modes of the pyrrole ligand are explicitly considered for all optimized geometries, viz., a η^5- and σ-bonded pyrrole. In addition, a stripped-down model, consisting of only a Cl atom as anionic fragment, and a full model, consisting of ClAlMe$_3$ as anion, are investigated for both bonding modes of pyrrole. Geometries for the Cl models will be designated as **H*x*** and **S*x*** for the respective η^5- and σ-bonding modes of pyrrole, while the designations **H*x*′** and **S*x*′** will be used for the ClAlMe$_3$ models. In this section the geometrical results obtained for the Cl models will be presented first, followed by a brief comparison of differences in geometries obtained upon changing from the Cl model to the full ClAlMe$_3$ model.

The optimized geometries for η^5-bonded pyrrole (Cl model) participating in the proposed ethylene trimerization mechanism are illustrated in Figure 4, while the corresponding σ-bonded pyrrole geometries are illustrated in Figure 5. The Cr(II) species **H1** is considered as the first active intermediate in the trimerization cycle. The optimized structure exhibits tetrahedral geometry with Cr−Py and Cr−Cl distances of 1.927 and 2.266 Å, respectively. The Cr center is in the plane defined by the four carbon atoms of the bonded ethylene molecules, and each ethylene molecule is weakly coordinated to Cr via π-bonding interaction. The relatively weak nature of the π-bonding is reflected in the relatively short C−C bond distance of 1.381 Å, which is only 0.045 Å longer than the calculated C═C distance in free ethylene. Furthermore, the Cr−C distances for a single ethylene fragment is not symmetrical, 2.245 and 2.331 Å, respectively, with the carbon atom designated for coupling with the other ethylene fragment exhibiting the longest Cr−C distance. The calculated Cr−N distance in **S1** is 1.904 Å, and the Cl ligand, as well as the two ethylene fragments, is more tightly coordinated to Cr compared to **H1**. This relatively contracted nature of the ligands is attributed to a higher demand for electron density by Cr when pyrrole is bonded in a σ-mode, in accord with the coordinatively unsaturated nature of Cr for σ-pyrrole (vide infra). Another significant difference in the geometries of **H1** and **S1** is the more pronounced piano-stool geometry for the former, in which the Cl and ethylene fragments are bent away from the pyrrole ligand.

Formation of the five-membered metallacycle Cr(IV) species **H2** is afforded by oxidative addition of the two ethylene fragments via the transition structure **H1−2**. In **H1−2** the coupling C−C distance is decreased from 2.598 Å in **H1** to 1.898 Å, while contraction of the η^5-bonded pyrrole ring in the transition state is evident from the changes in Cr−Py distance from 1.927 Å → 1.912 Å → 1.968 Å in the sequence **H1** → **H1−2** → **H2**. The transition structure for metallacycle formation of the σ-bonded pyrrole model, **S1−2**, points to a significantly earlier transition state, as is evident from the relatively longer C−C coupling distance (2.034 Å) and larger C−Cr−C angle (123.4°) compared to **H1−2**. The five-membered metallacycle products, **H2** and **S2**, have C−C coupling distances of 1.529 and 1.536 Å, respectively, which is in agreement with the expected distance for C−C single bonds. For both **H2** and **S2** the Cr−Cl and Cr−Py distances are shorter for the Cr(IV) complexes compared to the distances obtained for the Cr(II) complexes **H1** and **S1**.

In order for ethylene trimerization to proceed, the incorporation of a third ethylene molecule is necessary. Interaction of ethylene with the five-membered metallacycle **H2** affords **H3**, in which the ethylene fragment is weakly coordinated via a long-range π-interaction. This is evident from the elongated Cr−C distances

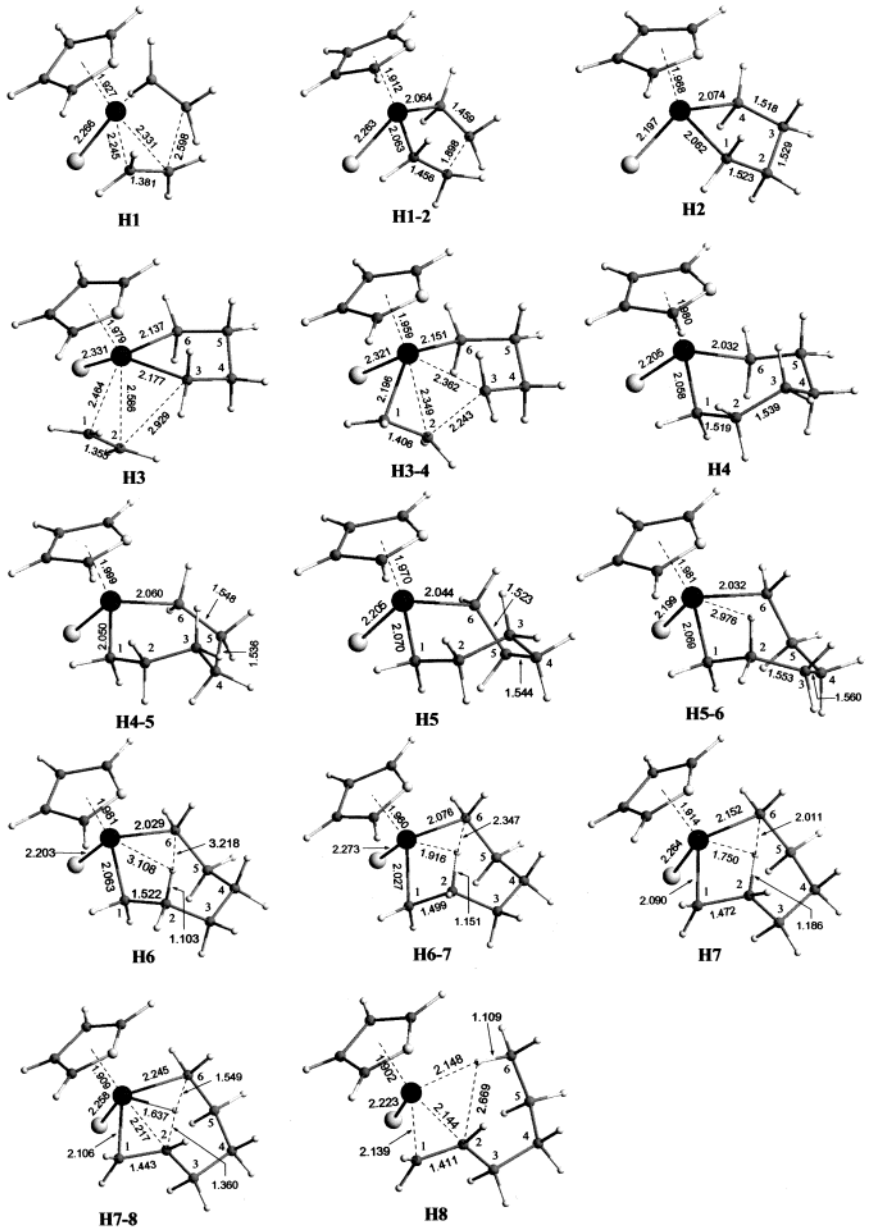

Figure 4. DMol^3/GGA/PW91/DNP optimized stationary points for η^5-pyrrole Cl models.

(2.464 and 2.586 Å) for Cr-ethylene in **H3**, as well as the relatively short C═C distance of 1.355 Å for the coordinated ethylene fragment. The significantly endothermic nature (vide infra) of ethylene coordination to **H2**, to yield the 16-electron species **H3**, corroborates the fact that Cr complexes tend to favor a low electron count in the valence shell. This is also evident from unsuccessful efforts to optimize a geometry similar to **H3** for σ-bonded pyrrole; each attempt led to the spontaneous dissociation of ethylene from the 10-electron species, **S2**, during optimization. It is therefore proposed that **H3** represents a shallow local minimum on the PES for effective concerted metallacycle growth from **H2** to **H4**. Insertion of the coordinated ethylene fragment into the Cr−C3 bond, and not the Cr−C6 bond, of **H3** is suggested from the elongated nature of Cr−C3 (2.177 Å) compared to Cr−C6 (2.137 Å). Metallacycle growth (**H3** → **H3**−**4** → **H4**) to yield the seven-membered metallacycle, **H4**, proceeds by insertion of ethylene into the Cr−C3 bond via the transition structure **H3**−**4**. In **H3**−**4** formation of the Cr−C1 (2.196 Å) and C2−C3 (2.243 Å) bonds and rupture of the Cr−C3 (2.362 Å) bond and C1−C2 (1.406 Å) π-bond proceed in a concerted fashion. In **H4** the Cr−C1 bond relaxes to 2.058 Å. A transition structure similar to **H3**−**4** was successfully optimized for a σ-bonded pyrrole complex (**S3**−**4**). In **S3**−**4** the C2−C3 distance (2.279 Å) is found to be similar compared to **H3**−**4**, while the Cr−C3 distance (2.181 Å) is significantly shorter and accompanied by an agostic interaction (2.012 Å) between Cr and a hydrogen on C3, which is not observed for **H3**−**4**. This additional bonding interaction found for the σ-bonded model reflects a comparative lack of electron density at the metal center in the transition state, which is not necessarily attributable to the relatively smaller formal number of valence electrons in **S3**−**4** compared to **H3**−**4** (see discussion for structure **H7**).

In order for the liberation of 1-hexene to proceed from the seven-membered metallacycles, **H4** and **S4**, reductive β-hydrogen migration from C2 to C6 (or from C5 to

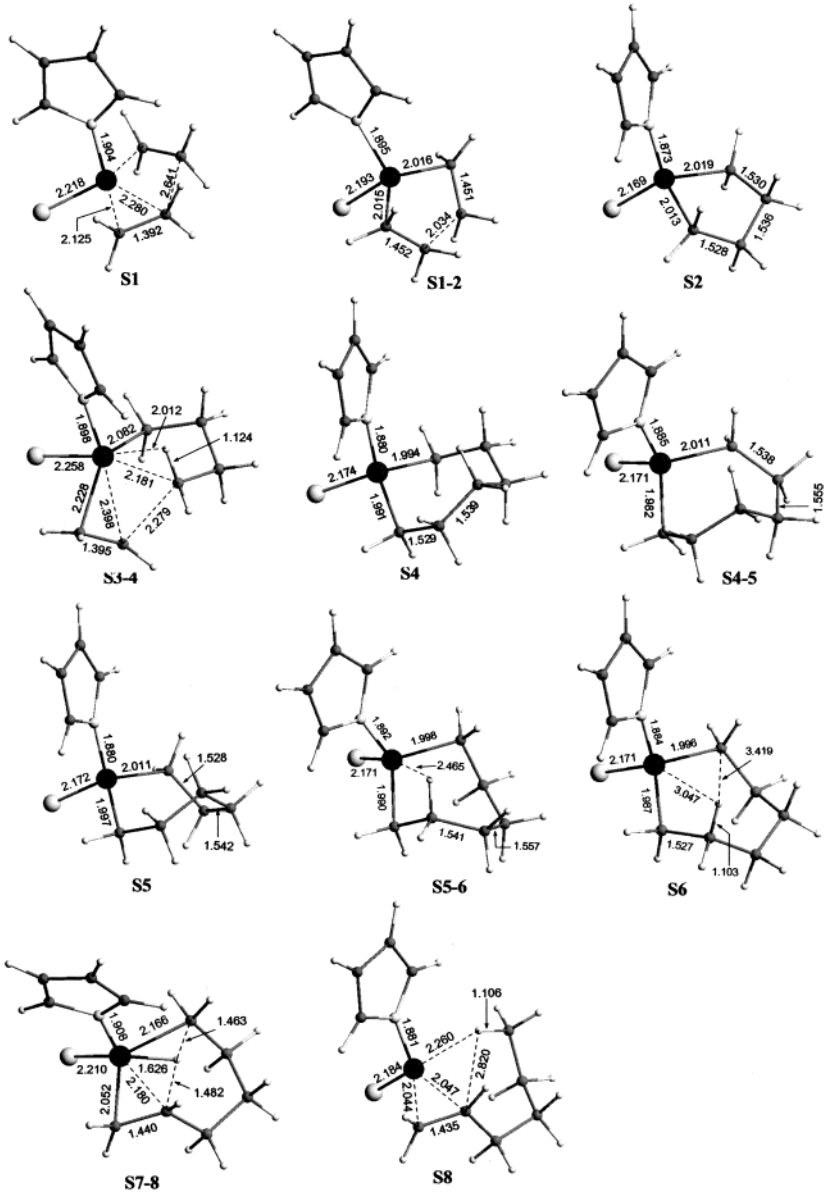

Figure 5. DMol^3/GGA/PW91/DNP optimized stationary points for σ-pyrrole Cl models.

C1) needs to take place. Inspection of the carbon backbone geometries in **H4** and **S4** reveals, however, that none of the β-hydrogens are ideally positioned to afford facile β-hydrogen migration. Sequential conformational changes from **H4** and **S4**, involving first an alteration at C5 (via transition structures **H4**−**5** and **S4**−**5** to yield **H5** and **S5**, respectively) and second an alteration at C3 (via transition structures **H5**−**6** and **S5**−**6** to yield **H6** and **S6**, respectively), afford seven-membered metallacycle geometries resembling boat conformations in which both C2 and C5 contain axial β-hydrogens suitable for β-hydrogen migration. In this mechanistic study migration of the axial β-hydrogen on C2 to C6 of **H6** and **S-6** was considered for all models.

Migration of the axial β-hydrogen of C2 in **H6** to C6 leads to the formation of an agostic intermediate structure **H7** via the transition structure **H6**−**7**. In **H6**−**7** the C2−H distance elongates to 1.151 Å, while the corresponding Cr−H, C1−C2, and H−C6 distances decrease to 1.916, 1.499, and 2.347 Å, respectively. The C2−H, Cr−H, C1−C2, and H−C6 distances relax to 1.186, 1.750, 1.472, and 2.011 Å, respectively, in the β-agostic intermediate **H7**. All attempts to optimize an agostic intermediate similar to **H7** for the σ-bonded pyrrole model was unsuccessful; each attempt resulted in the spontaneous formation of **S6**. This result is in contrast to the agostic interaction that was observed for σ-pyrrole in **S3**−**4**, but not for **H3**−**4**. Cr-mediated hydrogen migration from C2 in **H7** to C6, via the transition structure **H7**−**8**, yields 1-hexene coordinated to the resulting Cr(II) center (**H8**) via π-bonding interaction at the double bond and a remaining agostic interaction with the migrated hydrogen. Similar agostic-assisted hydrogen migration transition structures for ethylene trimerization with Ta and Ti catalysts were recently calculated and reported.[11,12] In **H7**−**8** the Cr−H (1.637 Å), C2−H (1.360), and C6−H (1.549 Å) distances suggest that the transition state is rather early and is more reactant (**H7**) like. This is in contrast to the Cr-mediated hydrogen migration transition structure optimized for the σ-bonded pyrrole model (**S7**−**8**) in which the Cr−H (1.627 Å), C2−H (1.482 Å), and C6−H (1.463 Å) distances suggest a later transition state than **H7**−**8**, which resembles the product (**S8**) more closely than

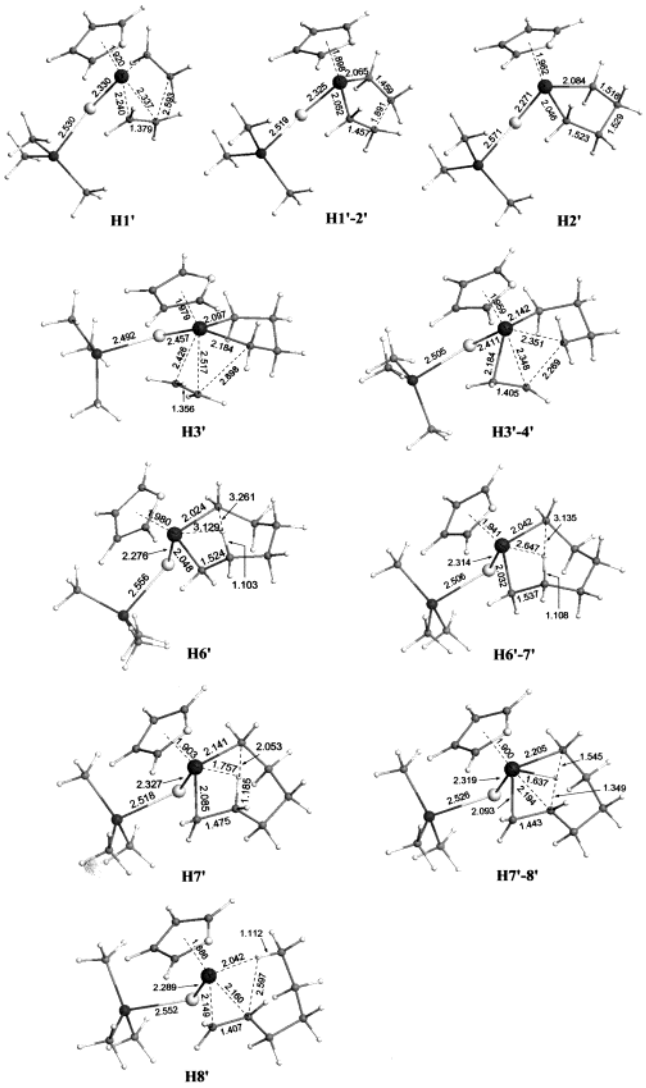

Figure 6. DMol^3/GGA/PW91/DNP optimized stationary points for η^5-pyrrole $ClAlMe_3$ models.

the reagent (**S6**). A significant decrease in Cr−Py distance upon following the sequence **H6** → **H6**−**7** → **H7** → **H7**−**8** → **H8** of 1.981 Å → 1.960 Å → 1.914 Å → 1.909 Å → 1.902 Å is found, effectively suggesting that contraction of the η^5-bonded pyrrole ring favors β-hydrogen migration. A similar decrease in Cr−N distance for **S6** → **S7**−**8** → **S8** is not found, which may relate to the significant differences found in activation energies for β-hydrogen migration for σ- and η^5-bonded pyrrole (vide infra).

Expansion of the Cl models to contain an anionic fragment consisting of trimethylaluminum chloride ($ClAlMe_3$) was considered for all geometries in the ethylene trimerization mechanistic sequence. A selection of optimized geometries for these expanded models is illustrated in Figures 6 and 7 for η^5- and σ-bonded pyrrole, respectively. Comparison of the optimized Cl model structure **H1** with the corresponding $ClAlMe_3$ model structure **H1′** shows elongation of the Cr−Cl distance by 0.064 Å and a Cl−Al coordination distance of 2.530 Å. The elongation of the Cr−Cl distance upon expansion of Cl to $ClAlMe_3$ is a general trend observed for all optimized geometries for both bonding modes of pyrrole. A slight decrease in coordination distances of the pyrrole ligand and two ethylene fragments is found between **H1** and **H1′**, which once again follows a consistent trend for Cr−ligand distances for all geometries considered in the mechanistic cycle. For most transition structures no significant geometrical differences are observed between the Cl and $ClAlMe_3$ models. However, a significantly less pronounced agostic interaction between Cr−H (2.388 Å) is observed for **S3′**−**4′** compared to **S3**−**4** (2.012 Å), which allows for a longer Cr−C3 (2.259 Å) and shorter Cr−C1 (2.113 Å) distance in **S3′**−**4′** compared to Cr−C3 (2.181 Å) and Cr−C1 (2.228 Å) in **S3**−**4**. The more favorable nature of the **S3′**−**4′** geometry compared to **S3**−**4** is reflected in the relatively lower activation energy observed in this step for the $ClAlMe_3$ model compared to the Cl model for σ-pyrrole (vide infra). Similarly, the relatively shorter C2−H distance (1.108 Å) and longer Cr−H distance (2.647 Å) in the transition structure **H6′**−**7′** compared to the corresponding distances in **H6**−**7** (1.151 and 1.916 Å, respectively) suggest that the former transition state ($ClAlMe_3$ model) is significantly earlier compared to the corresponding transition state for the Cl model. Nevertheless, most geometrical differences found for η^5- and σ-bonded pyrrole in the Cl models are effectively reproduced for the different bonding modes of pyrrole in the more realistic $ClAlMe_3$ models.

Electronic versus Gibbs Free Energies. The Cr(II) structures **H1**, **S1**, **H1′**, and **S1′** have been chosen as reference structures to which the energies of all stationary points in the mechanistic sequence are related and corrected with the relevant number of ethylene molecules. The DMol^3/GGA/PW91 potential energy surfaces (PESs) for the two Cl models and two $ClAlMe_3$ models, i.e., for η^5- and σ-bonded pyrrole in each case, are illustrated as four separate energy level diagrams in Figure 8. In each case the relative electronic energy differences (without the inclusion of zero-point energy corrections and designated as ΔE) and relative variations in calculated Gibbs free energy corrections to the electronic energies (with the inclusion of ZPE corrections), for all stationary points in the proposed mechanism, are illustrated. Two temperatures for the Gibbs free energy corrections, viz., 298.15 and 375.00 K, are considered for each graph and are designated by ΔG_{298} and ΔG_{375}, respectively.

A comparison of the electronic (ΔE) and Gibbs free energy (ΔG_{298} and ΔG_{375}) differences for *η^5-bonded pyrrole in the Cl model* (graph a in Figure 8) shows essentially no differences for the metallacycle formation sequence **H1** → **H1**−**2** → **H2**, for which similar activation (ΔE_a = 9.7, $\Delta G^{\ddagger}_{298}$ = 10.4, and $\Delta G^{\ddagger}_{375}$ = 10.7 kcal/mol, respectively) and reaction energies (ΔE = 2.0, ΔG_{298} = 1.9, and ΔG_{375} = 2.2 kcal/mol, respectively) are found. In contrast, however, the metallacycle growth sequence **H2** → **H3**−**4** → **H4** shows significant differences for both calculated activation (ΔE_a = 13.4, $\Delta G^{\ddagger}_{298}$ = 29.1, and $\Delta G^{\ddagger}_{375}$ = 32.9 kcal/mol, respectively) and reaction energies (ΔE = −20.9, ΔG_{298} = −5.6, and ΔG_{375} = −2.4 kcal/mol, respectively) between the relative electronic and Gibbs free energy values. The relatively less favorable reaction and activation Gibbs free energies are attributable to unfavorable entropy ($T\Delta S$) corrections to the total electronic energies when an additional ethylene molecule is introduced to the mechanism and inserted into the five-membered metallacycle structure **H2** (vide

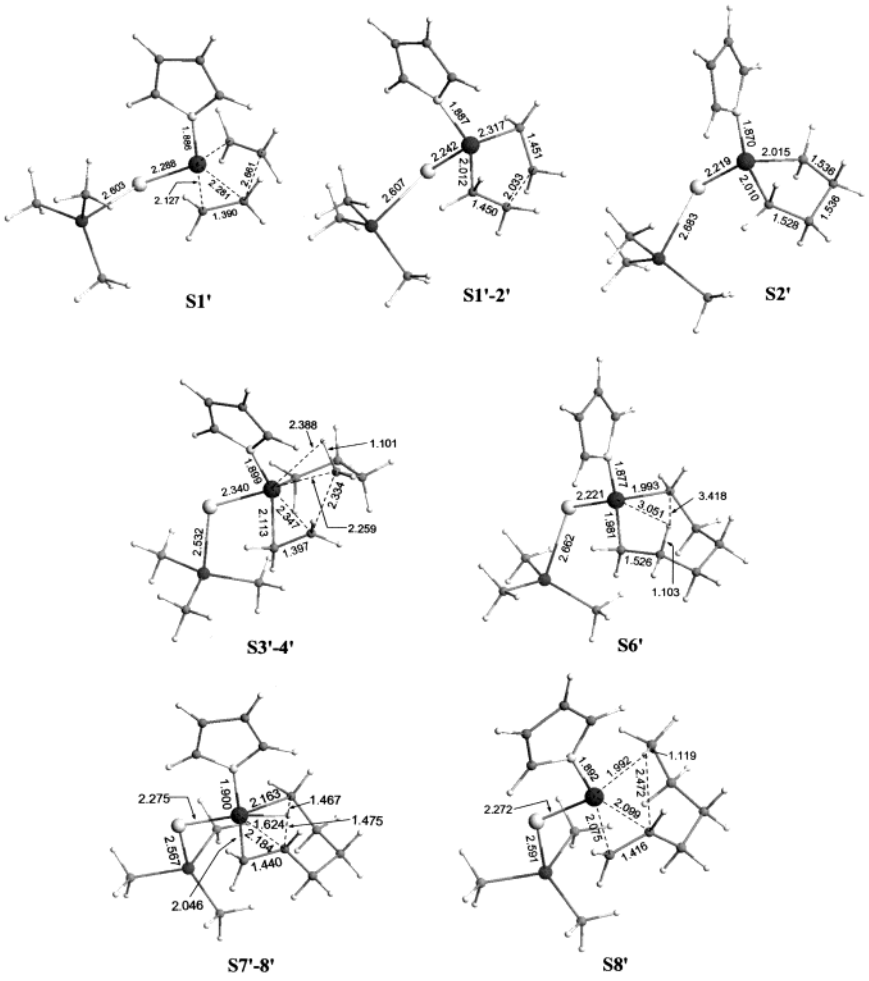

Figure 7. DMol^3/GGA/PW91/DNP optimized stationary points for σ-pyrrole $ClAlMe_3$ models.

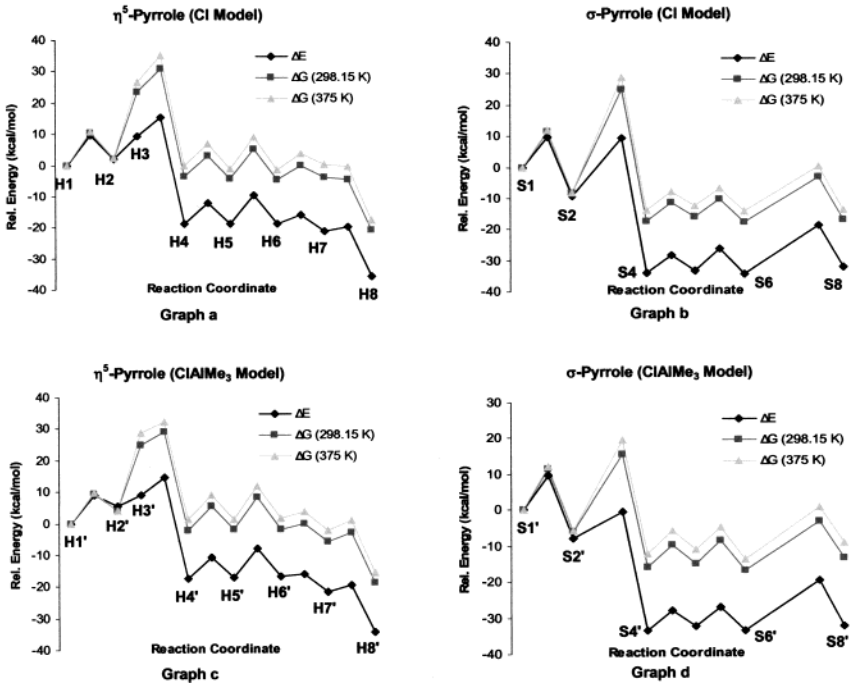

Figure 8. Comparative ΔE, ΔG_{298}, and ΔG_{375} DMol^3/GGA/PW91/DNP potential energy surfaces for η^5- and σ-pyrrole for both the stripped-down Cl and full $ClAlMe_3$ anion models.

infra). An essentially constant difference between calculated total electronic energies (ΔE) and Gibbs free energies (ΔG_{298} and ΔG_{375}) of ca. 15 and 18 kcal/mol, for ΔG_{298} and ΔG_{375}, respectively, is found to be maintained for the rest of the mechanistic sequence **H4** through **H8**.

Table 2. Reaction (ΔE, ΔH_{298}, $T\Delta S_{298}$, and ΔG_{298}) and Activation (ΔE_a, $\Delta H^{\ddagger}_{298}$, $T\Delta S^{\ddagger}_{298}$, and $\Delta G^{\ddagger}_{298}$) Parameters (kcal/mol) for Metallacycle Formation and Metallacycle Growth for Both the Cl and $ClAlMe_3$ Models

reaction step	ΔE	ΔE_a	ΔH	$\Delta H^{\ddagger}$	$T\Delta S$	$T\Delta S^{\ddagger}$	ΔG	$\Delta G^{\ddagger}$
H1 → H1−2 → H2	2.0	9.7	0.8	9.3	−1.1	−1.1	1.9	10.4
S1 → S1−2 → S2	−9.3	9.6	−9.1	9.7	−0.7	−1.6	−8.4	11.3
H1′ → H1′−2′ → H2′	5.5	9.1	4.6	9.1	0.5	−0.4	4.0	9.5
S1′ → S1′-2′ → S2′	−8.0	9.5	−7.4	9.4	−1.2	−2.0	−6.2	11.4
H2 → H3−4 → H4	−21.0	13.4	−17.9	14.6	−12.4	−14.5	−5.6	29.1
S2 → S3−4 → S4	−24.7	18.7	−22.2	19.2	−13.2	−14.0	−9.1	33.2
H2′ → H3′−4′ → H4′	−23.1	9.2	−20.4	11.1	−14.1	−13.9	−6.3	25.0
S2′ → S3′−4′ → S4′	−25.7	7.3	−22.6	8.3	−12.8	−13.6	−9.8	21.8

Calculated reaction and activation electronic energies (ΔE), as well as the corresponding enthalpy (ΔH), entropy ($T\Delta S$), and Gibbs free energy (ΔG) corrections at 298.15 K, for metallacycle formation and metallacycle growth (for both the Cl and $ClAlMe_3$ models and both bonding modes of pyrrole) are summarized in Table 2. From Table 2 it is evident that the $T\Delta S_{298}$ contributions to the calculated Gibbs free energies for metallacycle formation is negligible (−1.1 to 0.5 kcal/mol), which relates to the similar metallacycle formation ΔH_{298} and ΔG_{298} values according to the relation $\Delta G = \Delta H - T\Delta S$. In contrast, however, relatively large negative $T\Delta S_{298}$ contributions (−14.1 to −12.4 kcal/mol) to ΔG_{298} for metallacycle growth are found. A similar trend is observed for the relative calculated activation energy parameters in which the $T\Delta S^{\ddagger}_{298}$ contributions to $\Delta G^{\ddagger}_{298}$ are negligible for metallacycle formation (−2.0 to −0.4 kcal/mol), but significantly negative for metallacycle growth (−14.5 to −13.6 kcal/mol). These unfavorable entropy contributions arise from the incorporation of an additional ethylene molecule during metallacycle growth, essentially converting a bimolecular system to a unimolecular system. The effective Gibbs free energies of activation ($\Delta G^{\ddagger}_{298}$) for metallacycle growth, in, for example, the $ClAlMe_3$ sequence **H2′ → H3′−4′**, show that consideration of only electronic energy differences would lead to a 15.8 kcal/mol underestimation of the activation energy determined for $\Delta G^{\ddagger}_{298}$ and serves to emphasize the importance of inclusion of free energy corrections to the calculated energy differences. A similar increase in the estimation of the effective metallacycle growth activation energy by 11.3 kcal/mol, upon inclusion of thermodynamic corrections at 298.15 K, is reflected in the recently reported DFT study on Ti-catalyzed ethylene trimerization by de Bruin et al.[11b]

A general comparison of the graphs in Figure 8 shows that an increase of temperature from 298.15 to 375 K has no significant effect on calculated Gibbs free energy differences for metallacycle formation. Metallacycle growth is, however, calculated to proceed with a slightly higher activation energy for all four mechanisms represented in Figure 8. This increase in $\Delta G^{\ddagger}_{375}$ compared to $\Delta G^{\ddagger}_{298}$ results from an increase in the negative entropy contribution ($T\Delta S^{\ddagger}_{375}$) to $\Delta G^{\ddagger}_{375}$ relative to the $T\Delta S^{\ddagger}_{298}$ contribution to $\Delta G^{\ddagger}_{298}$ (not included in Table 2).

The relatively constant ΔG correction ratios obtained for the different models are evident from the similar graphs in Figure 8. Consequently, the Gibbs free energy differences at 298.15 K (ΔG_{298}) will be used for all energy and mechanistic comparisons among stationary points in the remainder of this paper. The relative energies for η^5- and σ-bonded pyrrole will be compared for the *Cl model*, followed by a brief discussion on the differences obtained with expansion to the *$ClAlMe_3$ model*. Comparative PESs (ΔG_{298}) for η^5- and σ-bonded pyrrole are illustrated in Figures 9 and 10 for the Cl and $ClAlMe_3$ models, respectively. Note that in each case the energies of all stationary points are referenced to the respective calculated ΔG_{298} values for **H1** (Figure 4) and **H1′** (Figure 6).

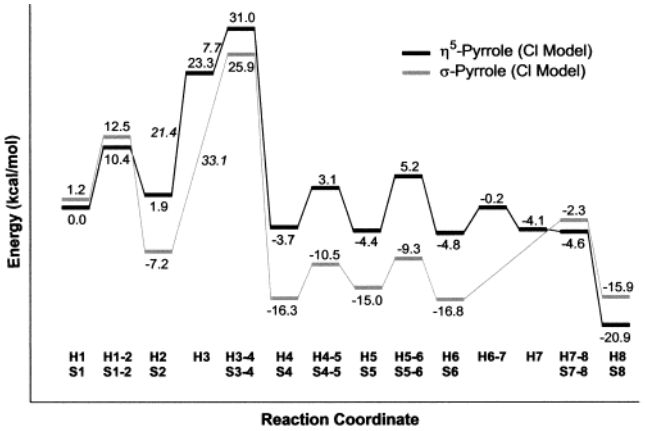

Figure 9. Relative ΔG_{298} DMol^3/GGA/PW91/DNP potential energy surfaces for η^5- and σ-pyrrole for the Cl anion models (kcal/mol). All energies are relative to **H1** corrected with the relevant number of ethylene molecules. Energy differences between two stationary points are indicated in italics.

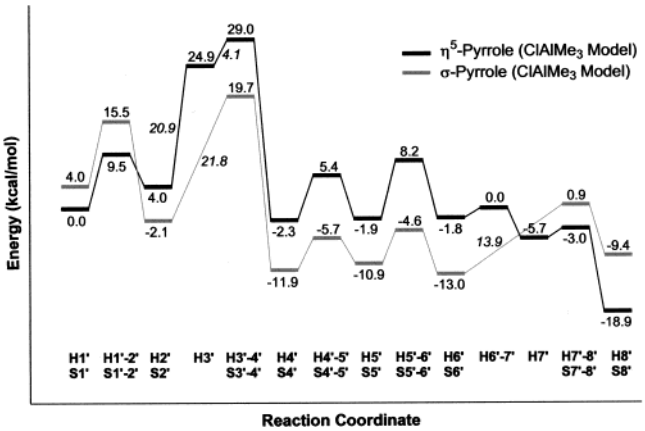

Figure 10. Relative ΔG_{298} DMol^3/GGA/PW91/DNP potential energy surfaces for η^5- and σ-pyrrole for the $ClAlMe_3$ anion models (kcal/mol). All energies are relative to **H1′** corrected with the relevant number of ethylene molecules. Energy differences between two stationary points are indicated in italics.

η^5- versus σ-Bonded Pyrrole: Metallacycle Formation. Metallacycle formation for η^5-bonded pyrrole from **H1** to **H2** (Figure 4) is calculated to be endothermic

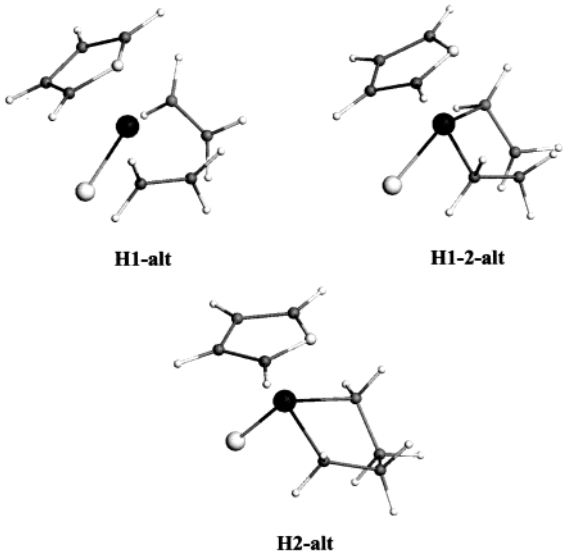

Figure 11. DMol^3/GGA/PW91/DNP optimized structures of **H1**−**alt**, **H1**−**2**−**alt**, and **H2**−**alt**.

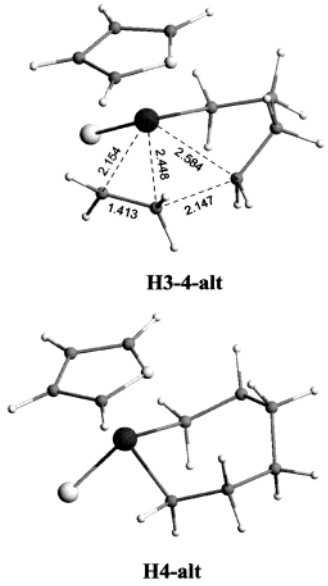

Figure 12. DMol^3/GGA/PW91/DNP optimized structures of **H3**−**4**−**alt** and **H4**−**alt**.

by 1.9 kcal/mol and requires a modest activation barrier, via transition structure **H1**−**2** (Figure 4), of 10.4 kcal/mol (Figure 9). The preferred conformation of the five-membered ring of **H2** is dictated by the relative orientation of the ethylene fragments in **H1** and **H1**−**2**. Alternative conformations for **H1**, **H1**−**2**, and **H2** were also optimized and are illustrated as **H1**−**alt**, **H1**−**2**−**alt**, and **H2**−**alt** in Figure 11. The calculated changes in ΔG_{298} for **H1** → **H2** and **H1** → **H1**−**2**−**alt** are 1.8 and 10.9 kcal/mol, respectively, which is essentially similar to the energies calculated for **H1** → **H2** and **H1** → **H1**−**2**. It was consequently decided to only consider the conformation as represented for **H2** as active intermediate in the mechanistic cycle. The metallacycle precursor for σ-bonded pyrrole, **S1** (Figure 5), is 1.2 kcal/mol higher (Figure 9) in energy compared to **H1**, which suggests that the η^5-bonded mode of pyrrole will thermodynamically be favored at the start of the mechanism. The comparative activation energy for metallacycle formation for σ-bonded pyrrole is slightly higher (11.3 kcal/mol) compared to η^5-bonded pyrrole (10.4 kcal/mol), which is in contrast to the significantly more favorable reaction energy for **S1** → **S2** (−8.4 kcal/mol) compared to **H1** → **H2** (1.9 kcal/mol). Consequently, **S2** is 9.1 kcal/mol lower in energy than **H2**, which suggests that the σ-bonded mode of pyrrole will thermodynamically be favored for the five-membered metallacycle. Formation of the five-membered metallacycle involves an oxidative addition process in which the oxidation state of Cr formally changes from II to IV.

***η*^{5}-versus*σ*-Bonded Pyrrole: Metallacycle Growth.** At this stage of the mechanism a competition between metallacyclopentane (**H2** and **S2**) decomposition, to yield 1-butene, and metallacycle growth upon incorporation of an additional ethylene molecule may be envisaged. However, 1-butene formation from metallacyclopentanes was found to be disfavored compared to metallacycle growth in theoretical studies for Ti-[11] and Ta-catalyzed[12] ethylene trimerization. In these studies it was found that 1-butene liberation from the metallacyclopentanes proceeds in a two-step mechanism which requires higher activation and reaction energies compared to metallacycle growth. These relatively unfavorable energies are attributed to the ring strain of the metallacyclopentanes. Therefore, reaction steps for competing 1-butene liberation from either **H2** and **S2** were not considered in this study.

In order for metallacycle growth to occur from **H2** an additional ethylene molecule needs to interact with Cr. Ethylene coordination to Cr in **H2** leads to the formation of the weak π-complex **H3** and is found to be significantly endothermic by 21.4 kcal/mol (Figure 9). This relatively high endothermicity is attributable to two factors, viz., an unfavorable entropy contribution to the Gibbs free energy for this step in the mechanism and the unprecedented nature of seven-coordinated Cr complexes mentioned to earlier (vide supra). Consequently, **H3** is regarded as a shallow local minimum on the path of effective concerted ethylene insertion in the Cr−C1 bond of **H2**. All efforts to optimize a σ-pyrrole complex similar to **H3** resulted in the spontaneous dissociation of the ethylene fragment from the complex, essentially suggesting that incorporation of ethylene in **S2** will be less favorable compared to incorporation of ethylene in **H2**. Once again, the coordination mode of the pyrrole ligand seems to dictate this discrepancy.

The relatively longer Cr−C2 distance (2.586 Å), compared to Cr−C1 (2.464 Å) in **H3**, as well as the relatively longer Cr−C3 (2.177 Å) versus Cr−C6 (2.137 Å) distance, suggest coordination of C2 with C3 during metallacycle growth. A transition structure (**H3**−**4**) for C2−C3 coordination in **H3** connects **H3** and **H4** with a barrier of 7.7 kcal/mol and an exothermicity of 27.0 kcal/mol. Alternative coordination of C1 and C3 in **H3** was also considered and leads to the formation of the transition structure **H3**−**4**−**alt** and seven-membered metallacycle product **H4**−**alt** illustrated in Figure 12. The increase in energy for **H3** → **H3**−**4**−**alt**, however, is 6.9 kcal/mol higher compared to **H3** → **H3**−**4**, making this mode of ethylene insertion less probable. The effective gain in energy for metallacycle growth **H2** + ethylene → **H4** is 5.6 kcal/mol with an effective activation barrier (**H2** + ethylene → **H3**−**4**) of 29.1 kcal/mol, essentially representing the rate-determining step in the η^5-pyrrole mechanism (Figure 9). This estimated barrier

is slightly higher than the barrier reported (23.3 kcal/mol) for the similar effective transformation in the calculated Ti-catalyzed trimerization of ethylene.[11b]

The sequence **S1** → **S3**−**4** → **S4** proceeds with an activation barrier of 33.1 kcal/mol, for concerted insertion of ethylene into the Cr−C1 bond of **S2** (Figure 5), and is exothermic by 9.1 kcal/mol. This metallacycle growth activation barrier represents the rate-determining step for the σ-pyrrole mechanism. A direct comparison of the relative energies for **H3**−**4** and **S3**−**4** (Figure 9) shows that **S3**−**4** is lower in energy than **H3**−**4** by 5.1 kcal/mol. This effectively suggests that the σ-coordinated pyrrole geometry will preferentially populate the transition state for metallacycle growth in the proposed mechanism. It is interesting to note that an agostic interaction between Cr and a hydrogen on C3 is present in **S3**−**4**, accompanied by a relatively short Cr−C3 distance, not found for **H3**−**4**. A σ-bonded mode of pyrrole is also preferred for the seven-membered metallacycle product, **S4**, which is found to be 12.6 kcal/mol lower in energy compared to **H4**.

η^5- versus σ-Bonded Pyrrole: 1-Hexene Liberation. 1-Hexene liberation from the direct metallacycle growth products, **H4** and **S4** (Figures 4 and 5), could in principle proceed by reductive β-hydrogen migration from C2 to C6 (or similarly from C5 to C1). None of the β-hydrogens in **H4** and **S4** do, however, have a preferred axial orientation necessary to ensure facile β-hydrogen migration. Consequently, the potential energy surfaces of these seven-membered metallacycle intermediates were investigated in more detail by considering additional conformations of the seven-membered ring. Downward rotation of C5 in **H4** (and **S4**) via transition structure **H4**−**5** (and **S4**−**5**) leads to the formation of the metallacycle intermediate **H5** (and **S5**), in which one of the β-hydrogens on C5 is positioned in a formal axial orientation. The activation energies for the conformational changes **H4** → **H5** and **S4** → **S5** are 6.8 and 5.8 kcal/mol, respectively, with reaction energies −0.7 and 1.3 kcal/mol, respectively. A second subsequent conformational change considered involves the downward rotation of C3 in **H5** (and **S5**), via transition structure **H5**−**6** (and **S5**−**6**), to yield the semi-chair geometry **H6** (and **S6**). The activation energies for this second conformational change are 9.6 and 5.6 kcal/mol for the respective η^5- and σ-bonded modes of pyrrole, with respective reaction energies of −0.4 and −1.8 kcal/mol. After this second conformational change a β-hydrogen on C-2 in **H6** (and **S6**) is formally axial, representing a conformation suitable for β-hydrogen migration from C2. The semi-chair conformations for the seven-membered rings in **H6** and **S6** are distinguished from the other conformations (**H4**, **H5**, **S4**, and **S5**) by the sequential *trans* orientations of axial hydrogens upon following the sequence C1 to C6 and are analogous to the lowest energy chair conformation for cyclohexane. Similar semi-chair conformations for seven-membered metallacycle structures were also explicitly considered in calculated ethylene trimerization mechanisms catalyzed by Ti[11] and Ta.[12] The relatively lower energies obtained for all σ-bonded pyrrole seven-membered metallacycles, as well as relatively lower activation energies for conformational changes, compared to the η^5-modes, suggest that the σ-bonding mode of pyrrole will be preferred in this region of the potential energy surface.

Although β-hydrogen migration may proceed from either C2 or C5 to C6 and C1 (in **H6** and **S6**), respectively, only the migration from C2 to C6 was considered in this mechanistic study. Significant energy differences are not envisaged for alternative β-hydrogen migration from C5 to C1. β-Hydrogen migration in **H6** leads to the formation of an agostic stabilized intermediate, **H7**, via the transition structure **H6**−**7**, with a low barrier of 4.6 kcal/mol and a reaction energy of 0.7 kcal/mol. Subsequent continuation of Cr-mediated β-hydrogen migration from **H7** proceeds via the transition structure **H7**−**8**, which is calculated to be 0.5 kcal/mol lower in energy than **H7**.[32] β-hydrogen migration involves reductive elimination of the Cr(IV) **H6** species to the corresponding Cr(II) species, **H8**, in which the liberated 1-hexene fragment is coordinated to Cr via a π-interaction at the double bond and an agostic interaction with the migrated hydrogen of C6. To ascertain whether the formation of the agostic intermediate geometry, **H7**, is a prerequisite for the transformation **H6** → **H8**, an intrinsic reaction path (IRP) calculation involving **H6** (reactant), **H7**−**8** (transition structure), and **H8** (product) was performed. From the PES mapped by the IRP calculation it was found that **H7**−**8** is directly connected to the product **H8**. In contrast, however, an additional equilibrium geometry between **H6** and **H7**−**8** was identified that corresponded to **H7**. This result emphasized that a stepwise pathway **H6** → **H7** → **H8** operates for η^5-pyrrole in this region of the PES, in contrast to the results obtained for σ-pyrrole (vide infra). The energy gain for the transformation **H7** → **H8** is 16.8 kcal/mol, while the gain in energy for the sequence **H6** → **H8** is 16.1 kcal/mol.

Similar Cr-mediated β-hydrogen migration in **S6** was calculated to proceed in a concerted fashion via the transition structure **S7**−**8** to the 1-hexene complex **S8**. No agostic stabilized intermediate for the σ-bonded pyrrole model, similar to **H7**, was successfully optimized, which is in contrast to the agostic interaction found for **S3**−**4**, but not for **H3**−**4**. IRP calculations for **S6** (reactant), **S7**−**8** (transition structure), and **S8** (product) confirmed that **S7**−**8** is directly connected to both **S6** and **S8**. Another interesting observation from this IRP calculation was that rotation of the pyrrolyl fragment in **S7**−**8** relative to the pyrrolyl orientation in **S6** and **S8** takes place spontaneously (Figure 9). Several efforts to optimize a transition state geometry that resembles the pyrrolyl orientation in **S6** and **S8** were unsuccessful; in each instance the transition state search converged to the **S7**−**8** geometry. The energy barrier for the transformation **S6** → **S8** is 14.5 kcal/mol, which is significantly higher than the effective barrier for **H6** → **H8** (4.6 kcal/mol). In addition **S6** → **S8** is endothermic by 0.9 kcal/mol, which is in sharp contrast to the exothermic transformation of **H6** → **H8** by 16.1 kcal/mol. The relatively lower energy of **H8** compared to **S8** (by 5.0 kcal/mol) represents one of the few areas

(32) The lower ΔG_{298} energy of **H7**−**8** compared to **H7** is explained by the relative thermodynamic corrections to the electronic energies of the respective species. Consideration of purely electronic energies shows that the energy of **H7**−**8** is 1.5 kcal/mol higher in energy compared to **H7**. The total correction to the electronic energy at 298.15 K for **H7**−**8** is 15.1 kcal/mol, whereas the corresponding correction for **H7** is 17.1 kcal/mol.

on the potential energy surface where a η^5-bonded pyrrole intermediate is more stable than the corresponding σ-mode. In general this suggests that the Cr(II) intermediates prefer a η^5-bonding mode of pyrrole, whereas the Cr(IV) intermediates prefer the alternative σ-bonding mode of pyrrole.

A significant feature of the transition structures **H7**−**8** and **S7**−**8** is the partial coordination of the migrating hydrogen to the Cr center, effectively emphasizing a migration process which is Cr-mediated. Similar agostic assisted hydrogen migration mechanisms were reported by Yu et al.,[12] Blok et al.,[11a] and de Bruin et al.[11b] for 1-hexene liberation in Ta- and Ti-catalyzed ethylene trimerization.

The selectivity toward 1-hexene in the ethylene trimerization mechanism is regulated by the relative activation energies for competing β-hydrogen migration in **H6** and **S6** compared to coordination and insertion of an additional (fourth) ethylene molecule in **H6** and **S6**. From theoretical studies on Ti[11] and Ta[12] it was found that ethylene coordination and insertion in respective metallacycloheptane intermediates are unfavorable compared to metallacycloheptane decomposition to yield 1-hexene. Ethylene coordination and insertion in metallacyclopentane inetermediates (**H2** and **S2**) is found to be particularly unfavorable in the current study. In addition, the relative activation energies for β-hydrogen migration in **H6** and **S6** are favorable. Consequently, a mechanism involving further metallacycle growth, to yield metallacyclononane intermediates and 1-octene liberation, is not envisaged to be energetically favorable and was not considered in the current study.

General inspection of the potential energy surface depicted in Figure 9 shows the overall ethylene trimerization transformations, **H1** + ethylene → **H8** and **S1** + ethylene → **S8**, are exothermic by −20.9 and −17.0 kcal/mol, respectively. This is in agreement with the fact that Cr-catalyzed trimerization is a facile process. The rate-determining step in the mechanism is predicted to be metallacycle growth with $\Delta G^{\ddagger}_{\text{overall}} = 38.2$ and 33.1 kcal/mol for η^5- and σ-bonded pyrrole, respectively. These $\Delta G^{\ddagger}_{\text{overall}}$ values are both related to the σ-pyrrole metallacyclopentane geometry, **S2**, in Figure 9. This is because the η^5-pyrrole metallacyclopentane, **H2**, which is higher in energy than **S2** by 9.1 kcal/mol, is in rapid equilibrium with the reference state **S2**.

ClAlMe$_3$ Models. Expansion of the Cl anion fragment to a more realistic $ClAlMe_3$ anionic fragment was deemed necessary to ensure closer resemblance of the theoretical models to actual reagents used in experimental studies. The comparative potential energy surfaces for the proposed ethylene trimerization mechanism for the η^5-bonding mode of pyrrole is illustrated in Figure 13 for both the Cl and $ClAlMe_3$ models. Excellent agreement of calculated activation and reaction energies is evident for the two models. The comparative potential energy surfaces for the σ-bonding mode of pyrrole (for both the Cl and $ClAlMe_3$ models) are illustrated in Figure 14. In contrast with the good agreement observed for η^5-bonded pyrrole models (Figure 13), a conspicuous lower activation energy for **S2′** → **S3′**−**4′** → **S4′** (21.8 kcal/mol) compared to **S2** → **S3**−**4** → **S4** (33.1 kcal/mol) is evident from Figure 14. This

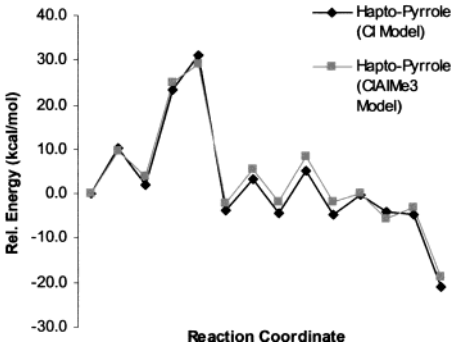

Figure 13. Relative ΔG_{298} DMol^3/GGA/PW91/DNP potential energy surfaces for η^5-pyrrole Cl and $ClAlMe_3$ anion models (kcal/mol).

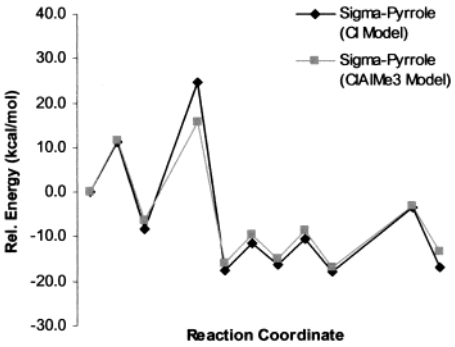

Figure 14. Relative ΔG_{298} DMol^3/GGA/PW91/DNP potential energy surfaces for σ-pyrrole Cl and $ClAlMe_3$ anion models (kcal/mol).

difference is attributed to significant geometrical differences found for the optimized structures of **S3′**−**4′** and **S3**−**4**, alluded to earlier, in which the $ClAlMe_3$ fragment in **S3′**−**4′** enforces significant relative elongation of the Cr−Cl bond, which in turn results in more favorable accommodation of the inserting ethylene fragment. This significant lowering of the activation energy for metallacycle growth, upon expansion of the anion fragment from Cl to $ClAlMe_3$, represents a fundamental lowering of the barrier of the rate-determining step in the overall proposed mechanism. This could in part point to the positive effect trialkylaluminums have on the Cr-catalyzed ethylene trimerization.

Ring Slippage. In Figure 9 the relative energies of all equilibrium and transition state geometries are presented, for both η^5- and σ-bonding modes of pyrrole, relative to the energy of the η^5-bonded structure **H1**. From this representation a direct energy comparison between similar structures with different bonding modes for pyrrole may be made. As pointed out earlier, metallacycle formation is preferred for the **H1** → **H1**−**2** → **H2** sequence due to the lower relative energy of **H1** versus **S1**, as well as the slightly lower activation energy necessary for metallacycle formation to proceed from the former. The significantly lower energy of **S2** compared to **H2** suggests, however, that a transformation from **H2** to **S2** will be favored on thermodynamic grounds. Such a transformation may be realized through a ring slippage mechanism in which the bonding mode of pyrrole formally changes from η^5 to σ. The concept of ligand ring slippage in organometallic chemistry, especially with reference to $\eta^5 \leftrightarrow \eta^3$ haptotropic shifts for

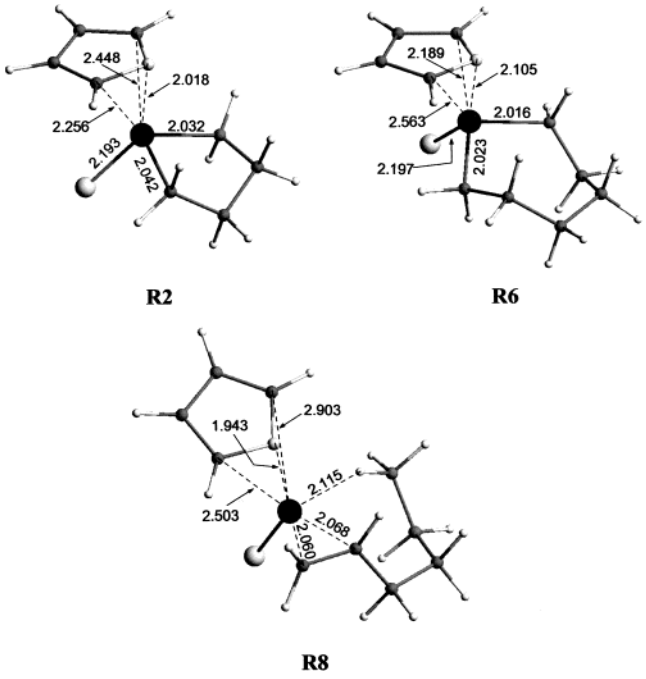

Figure 15. DMol³/GGA/PW91/DNP optimized structures of **R2**, **R6**, and **R8**.

cyclopentadienyl and indenyl ligands,[33] is well documented. Experimental studies by Kershner and Basolo[34] on η^5-heterocyclic manganese tricarbonyl complexes also suggest that pyrrole ring slippage is more facile compared to the isoelectronic cyclopentadienyl ligand. Recently, theoretical studies by Veiros[35] on pyrrolyl Mn complexes showed that pyrrole ring slippage essentially occurs between η^5- and σ-bonding modes, with no local minimum found for a η^3-bonding mode. This is in contrast to the preferred $\eta^5 \leftrightarrow \eta^3$ bonding mode changes observed for cyclopentadienyl derivatives.

Three areas on the potential energy surface displayed in Figure 9 were identified where ring slippage of the pyrrole ligand may have an impact on the calculated energetics, viz., the five-membered metallacycles (**H2** ↔ **S2**), the seven-membered metallacycles (**H6** ↔ **S6**), and the 1-hexene coordination complexes (**H8** ↔ **S8**). The transition structures for ring slippage between these equilibrium structures were successfully optimized and are illustrated as **R2**, **R6**, and **R8** in Figure 15 for **H2** ↔ **S2**, **H6** ↔ **S6**, and **H8** ↔ **S8**, respectively.

The coordination of pyrrole in **R2** resembles a distorted η^3-bonding mode in which the Cr−C2 (2.448 Å) and Cr−C5 (2.256 Å) distances are not similar[36] and the Cr−N distance (2.018 Å) is elongated compared to the Cr−N distance in **S2** (1.873 Å). As mentioned above, the metallacycle transition structure, **H1**−**2**, is energetically favored, and it is thus assumed that **H2** will be the direct metallacycle product. Transformation of **H2** to **S2**, via the ring slippage transition structure **R2**, is calculated to proceed with a low activation barrier of 2.6 kcal/mol and a gain in energy of 9.1 kcal/mol, as summarized in Table 3. This facile predicted change of bonding mode emphasizes the probability that the σ-pyrrole five-membered metallacycle is a thermodynamic sink in this area of the potential energy surface. Metallacycle growth necessarily then involves **S2**, and not **H2**, as the direct reagent structure. Insertion of ethylene into the Cr−C1 bond of **S2** is calculated to be a concerted process and proceeds with a rather high one-step activation barrier of 33.1 kcal/mol (Figure 9). Nevertheless, the lower relative energy of the σ-pyrrole metallacycle growth transition structure, **S3**−**4**, compared to the η^5-pyrrole counterpart, **H3**−**4**, suggests that the σ-coordination mode dominates in this region of the PES and that ring slippage prior or during metallacycle growth is unlikely (Figure 9).

Table 3. Calculated Activation and Reaction Gibbs Free Energies (298.15 K) for Selected Pyrrole Ring Slippage Transformations

ring slippage transformation	$\Delta G^{\ddagger}_{298}$ (kcal/mol)	ΔG_{298} (kcal/mol)
H2 → **S2**	2.6	−9.1
S2 → **H2**	11.7	9.1
H6 → **S6**	2.6	−12.0
S6 → **H6**	14.6	12.0
H6 → **S6**	10.9	5.0
S6 → **H6**	5.9	−5.0

The relatively lower energies of **S4**, **S5**, and **S6**, as well as the more favorable activation energies for conformational changes of the seven-membered metallacycles, compared to the η^5-analogues suggest that ring slippage of the pyrrole ring will most likely not be operating in this area of the potential energy surface. The relatively lower energy of the β-hydrogen migration transition structure **H7**−**8** compared to **S7**−**8** does, however, suggest that $\sigma \rightarrow \eta^5$ ring slippage in the most likely precursor, **S6**, is probable. The coordination of pyrrole in the transition structure for **S6** ↔ **H6** ring slippage, **R6** (Figure 15), involves a distorted η^3-bonding mode similar to the geometry of **R2**. The activation energy for the sequence **S6** → **R6** → **H6** is 14.6 kcal/mol and is endothermic by 12.0 kcal/mol (Table 3). This activation barrier should be compared to the competing mechanistic sequence **S6** → **S7**−**8** → **S8**, which proceeds with an almost identical activation energy of 14.5 kcal/mol (Figure 9). Consequently, no preference is found for ring slippage (**S6** → **H6**) or σ-pyrrole β-hydrogen migration on kinetic grounds. However, inspection of the relative energy profiles in Figure 9 reveals that the β-hydrogen migration barrier (for η^5-bonded pyrrole) is dictated by the activation barrier for formation of the agostic intermediate **H7**, from which subsequent 1-hexene liberation essentially proceeds without barrier. It is thus envisaged that β-hydrogen migration from **S6**, with concomitant ring slippage, will give prevalence to a direct mechanistic sequence **S6** → **H7**, which should not only represent the lowest energy path for β-hydrogen migration from **S6** but also provide for the formation of the thermodynamically more favored 1-hexene complex, **H8**. This reasoning is further supported by the significantly earlier nature of the transition state, **H7**−**8**, compared to **S7**−**8** (vide supra).

The earlier nature of **H7**−**8**, compared to **S7**−**8**, is related to the relative Cr−ligand distance flexibility in the proposed mechanism. In Figure 16 the relative Cr−

(33) O'Connor, J. M.; Casey, C. P. *Chem. Rev.* **1987**, *87*, 307.
(34) Kershner, D. L.; Basolo, F. *J. Am. Chem. Soc.* **1987**, *109*, 7396.
(35) Veiros, L. F. *J. Organomet. Chem.* **1999**, *587*, 221.
(36) This distorted η^3-coordination mode of the pyrrole ligand in **R2** may also be described as a distorted η^2-coordination mode in which N and one adjacent C in the pyrrole ring are mostly involved in the bonding. This effect is more pronounced in the geometries of **R6** and **R8**.

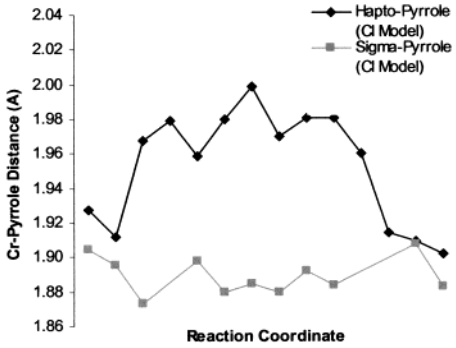

Figure 16. Variation in Cr−pyrrole distance for η^5- and σ-pyrrole (Cl model) along the reaction coordinate of the proposed mechanism.

pyrrole distances[37] for η^5- and σ-bonded pyrrole, for all stationary points (Figures 9 and 10), are plotted against the reaction coordinate. In general, it is found that whereas the Cr−σ-pyrrole distances show a maximum difference of 0.035 Å with no significant trend along the reaction coordinate, the Cr−η^5-pyrrole distances show a maximum difference of 0.097 Å and a definite trend related to the oxidation state of Cr. The Cr(II) species, **H1** and **H8**, exhibit relatively short Cr−pyrrole distances of 1.902 and 1.927 Å, whereas the Cr(IV) species have an average Cr−pyrrole distance of 1.975 Å. Upon following the mechanistic sequence **H6** → **H6**−**7** → **H7** → **H7**−**8** → **H8**, an incremental decrease in Cr−pyrrole distances of 1.981 → 1.960 → 1.914 → 1.909 → 1.902 Å is observed (Figure 16), effectively suggesting that a closer proximity of the η^5-bonded ring will favor the reductive eliminative β-hydrogen migration process. A similar Cr−pyrrole distance contraction is not observed during β-hydrogen migration of the σ-bonded pyrrole complex **S6** to **S8**. The apparently favorable contraction of the η^5-bonded pyrrole in the final stage of the proposed mechanism is also reflected in the relatively early nature of the transition structure **H7**−**8** compared to **S7**−**8**, in which a relatively short C2−H distance of 1.360 Å for the former is observed versus 1.482 Å for the latter.

The η^5-pyrrole 1-hexene coordination complex, **H8**, is 5.0 kcal/mol lower in energy compared to the corresponding σ-pyrrole complex, **S8**. Therefore, if the **S8** complex is the preferred direct 1-hexene coordination complex, ring slippage from **S8** to **H8** is likely, which is calculated to proceed with an activation barrier of 5.9 kcal/mol. Transformation of **H1** from **H8** by substitution of 1-hexene with 2 equiv of ethylene regenerates the first active intermediate in the proposed ethylene trimerization cycle.

Population Analysis. The calculated Hirshfeld charges located on Cr, the pyrrole ring,[38] and Cl for all stationary points on the potential energy surface of the Cl models are graphically illustrated in Figure 17. The average charges on Cr and pyrrole for the η^5-bonded pyrrole models in Figure 17 are 0.445 and −0.039 e, respectively, while the corresponding average charges

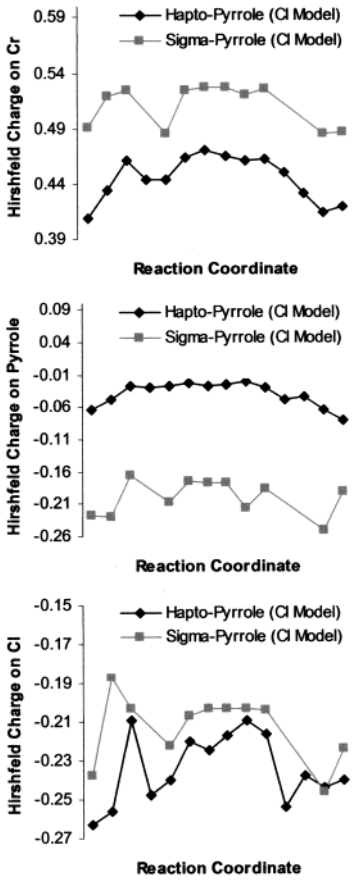

Figure 17. Relative DMol^3/GGA/PW91/DNP calculated Hirshfeld charges on Cr, pyrrole, and Cl for η^5- and σ-pyrrole (Cl model).

on Cr and pyrrole for the σ-bonded pyrrole models are 0.511 and −0.201 e, respectively. The slightly less positive charge on Cr and significantly less negative charge on pyrrole, for the η^5-bonded models compared to the σ-bonded models, suggest that the charge distribution between metal and ligand for the former is more dispersed compared to the latter. This effect is more pronounced between pyrrole and Cr for the two models than for Cr and Cl, as is evident from the similar average Hirshfeld charges on Cl for the η^5- (−0.234 e) and σ-bonded pyrrole (−0.213 e) models.

The Hirshfeld charges on Cr, with the exception of **H3**, **H3**−**4**, and **S3**−**4**, are related to the formal oxidation state of Cr. The Cr(II) complexes at the beginning and end of the proposed mechanism exhibit relatively smaller positive charges on Cr compared to the Cr(IV) complexes. This is in agreement with a less pronounced electron distribution at the Cr center for the Cr(IV) oxidation state compared to the Cr(II) oxidation state. The relative lowering in positive charge on Cr for **H3**, **H3**−**4**, and **S3**−**4** is qualitatively attributed to the introduction of additional electron density to the Cr center upon incorporation of a third ethylene fragment to the catalytic cycle. This lowering of charge on Cr is consistent with temporary expansion of coordination number of Cr for ethylene coordination (**H3**) and concerted ethylene insertion (**H3**−**4** and **S3**−**4**). It is also interesting to note that a good correlation between charge variation on Cr and distance between Cr and the η^5-bonded pyrrole ring (see Figure 16) exists.

(37) The Cr−pyrrole distances for η^5-bonded pyrrole refer to the distance of the Cr−pyrrole centroid axis, whereas the Cr−pyrrole distances for σ-bonded pyrrole refer to the Cr−N distances.

(38) The total Hirshfeld charge of the pyrrole ring is calculated by summation of all Hirshfeld charges located on the respective atoms in the ring.

Conclusions

In this theoretical contribution on Cr-catalyzed trimerization of ethylene a mechanism is proposed for the Phillips (Cr-pyrrolyl) trimerization catalyst system and energies for the different steps are calculated at the nonlocal DFT (DMol^3/GGA/PW91/DNP) level of theory. A detailed analysis to determine the preferred ground spin state for the active Cr(II) and Cr(IV) species in the mechanism was conducted. From these calculations it was determined that the triplet spin states for both Cr(II) and Cr(IV) are predicted to be the ground state at the GGA/PW91 level of theory. Both additional possible spin states for the Cr(II) species (singlet and quintet), as well as the singlet spin state for Cr(IV) species, were found to be significantly more unfavorable based on relative electronic energies. The main conclusion from these results was that spin state crossing during the proposed mechanism is unlikely to occur, effectively eliminating the necessity to locate minimum energy crossing points (MECPs) for the proposed mechanism. The proposed ethylene trimerization mechanism is based on the formation of metallacycle intermediates. Two important features of the proposed mechanism were explicitly investigated: first, the preferred coordination mode of the pyrrole ligand in each step of the mechanism, and second, the importance of expansion of a model Cl anion to a more realistic $ClAlMe_3$ anion fragment.

The calculated Gibbs free energy profiles at 298.15 K (Cl model) for the full potential energy surfaces of η^5- and a σ-coordinated pyrrole were both found to be favorable on thermodynamic grounds, with $\Delta G_{overall} = -20.9$ and -17.1 kcal/mol, respectively. The rate-determining step in the mechanism for both bonding modes of pyrrole was metallacycle growth from the corresponding metallacyclopentane reagent to the metallacycloheptane product with $\Delta G^{\ddagger}_{overall} = 38.2$ and 33.1 kcal/mol for η^5- and σ-bonded pyrrole, respectively. We have shown that the change of pyrrole bonding mode is an important concept in the proposed mechanism. A η^5-bonding mode of pyrrole is calculated to be favored for metallacycle formation, whereas a σ-bonding mode is favored for metallacycle growth and changes in conformations of seven-membered metallacycle intermediates. No preference was found for η^5- or σ-pyrrole in the final reductive eliminative liberation of 1-hexene in the proposed mechanism. Transition state geometries were calculated for pyrrole ring slippage ($\eta^5 \leftrightarrow \sigma$) for selected stationary points on the potential energy surface, which showed that the activation barrier for bonding mode change is small. These theoretical results thus suggest that facile change of pyrrole bonding mode enhances the catalytic efficiency of the Cr-pyrrolyl ethylene trimerization.

Potential energy surface calculations on the more realistic $ClAlMe_3$ anion models showed remarkable similarities to the PES obtained for the stripped-down Cl models. One important difference for calculated activation energy for metallacycle growth was, however, found for the σ-coordinated pyrrole models. A significant lowering of activation energy of the rate-determining step by 11.3 kcal/mol is found for the $ClAlMe_3$ model compared to the stripped-down Cl model in this step. This result suggests that the full aluminate anion may have an important role in controlling the reactivity of the Cr-pyrrolyl catalyst system.

Acknowledgment. We acknowledge Mr. Ivan Bester (Information Management, Sasol) for the efficient way in which he manages all technical software and hardware requirements of the Molecular Modeling department at Sasol Technology. We also wish to thank the members of the Sasol ethylene trimerization group for fruitful discussions and Sasol Technology Ltd for permission to publish this work.

Supporting Information Available: Cartesian coordinates for all optimized geometries. This information is available free of charge via the Internet at http://pubs.acs.org.

OM0306269